Available online at www.sciencedirect.com
ScienceDirect
Journal of Nuclear Materials 363–365 (2007) 570–574
journal of nuclear materials
www.elsevier.com/locate/jnucmat

Experimental and numerical studies of separatrix splitting and magnetic footprints in DIII-D

T.E. Evans [a,*], I. Joseph [b], R.A. Moyer [b], M.E. Fenstermacher [c], C.J. Lasnier [c], L.W. Yan [d]

[a] General Atomics, P.O. Box 85608, San Diego, CA 92186-5608, USA
[b] University of California at San Diego, 9500 Gilman Drive, La Jolla, CA 92093, USA
[c] Lawrence Livermore National Laboratory, Livermore, CA 94550, USA
[d] Southwestern Institute of Physics, P.O. Box 432, Chengdu, Sichuan, China

Abstract

A numerical field line integration code is used to study the structure of divertor footprints produced by small non-axisymmetric magnetic perturbations in the DIII-D tokamak. The modeling results are compared to experimental data which show a splitting of the divertor target plate heat flux into several distinct peaks when an $n = 3$ magnetic perturbation from the DIII-D I-coil is applied. The splitting consistently appears when the $n = 3$ perturbation is applied and disappears when the perturbation is removed. The magnitude of the splitting implied by the modeling is a factor of 2–3 smaller than the splitting seen in the experimental data. These results suggest that the plasma response to the applied $n = 3$ edge resonant magnetic perturbation amplifies the vacuum magnetic footprint structure on the divertor target plates. These results may have significant implications for the ITER divertor design.

PACS: 05.45.−a; 05.45.Pq; 28.52.−s; 52.55.Fa; 52.55.−s; 52.55.Rk; 52.25.Fi

Keywords: DIII-D; Edge modeling; ELM; Magnetic Topology; Stochastic boundary

1. Introduction

When subjected to small non-axisymmetric magnetic perturbations, the separatrix of a poloidally diverted tokamak is transformed from an axisymmetric 2D geometry into a set of intersecting invariant manifolds that define a somewhat more complex 3D topology [1]. We refer to this process as separatrix splitting and the patterns formed by the intersection of the invariant manifolds with solid surfaces as magnetic footprints. This process is unavoidable when non-axisymmetric magnetic perturbations, such as those from external correction/control coils, field-errors or internal magnetohydrodynamic (MHD) modes, are present in the system. These magnetic structures can have significant implications for the deposition of heat and particle fluxes on divertor structures and first wall

* Corresponding author. Fax: +1 858 455 4156.
E-mail addresses: evans@fusion.gat.com (T.E. Evans), ijoseph@ucsd.edu (I. Joseph).

0022-3115/$ - see front matter © 2007 Elsevier B.V. All rights reserved.
doi:10.1016/j.jnucmat.2006.12.064

components in regimes where parallel transport is comparable or greater than perpendicular transport and thus are of considerable interest for plasma–surface interaction research in toroidal fusion devices.

The mathematical theory of the structures formed due to separatrix or invariant manifold splitting in simple Hamiltonian systems, generically referred to as homoclinic tangles, has been extensively studied and is well understood [2–4]. The application of invariant manifold theory to magnetic field lines in realistic poloidally diverted tokamaks is most directly approached by numerical field line integration and mapping codes such as TRIP3D [5] and TRIP3D_MAP [6] where the unperturbed axisymmetric field is derived from experimentally constrained equilibria. These equilibria are calculated with the EFIT Grad-Shafranov code [7], that includes realistic plasma pressure and current profiles. In addition, mapping codes used to study simplified wire models of poloidally diverted tokamaks [8] are valuable for comparing the properties of field line trajectories to a broader class of dynamics generic to conservative vector field systems, i.e., Hamiltonian systems. Finally, as suggested by the present data, the response of the plasma to changes in the magnetic topology can be significant and may act to either amplify or reduce the effect of the splitting.

In this paper, we present measurements of heat flux and particle recycling patterns in the DIII-D lower divertor that are qualitatively consistent with the expected helical structure of magnetic footprints defined by homoclinic tangles produced during $n = 3$ I-coil experiments in DIII-D [9]. DIII-D data is presented in Section 2 and numerical modeling results from the TRIP3D field line integration code in Section 3. The experimental measurements and the numerical modeling are compared in Section 4.

2. Experimental background and observations

The separatrix splitting and magnetic footprint studies discussed in this paper are done with lower divertor target plate imaging diagnostics located at two toroidal angles using a dominantly lower null diverted plasma (Fig. 1(a)). The principle diagnostics are an infrared television (IRTV) [10] centered at a toroidal angle $\phi = 60°$, as shown in Fig. 1(a), and a downward tilted, tangentially aligned visible camera viewing D_α recycling light between $\phi = 120°$ and $\phi = 225°$ [11]. The IRTV is used to measure radial heat flux profiles across the lower

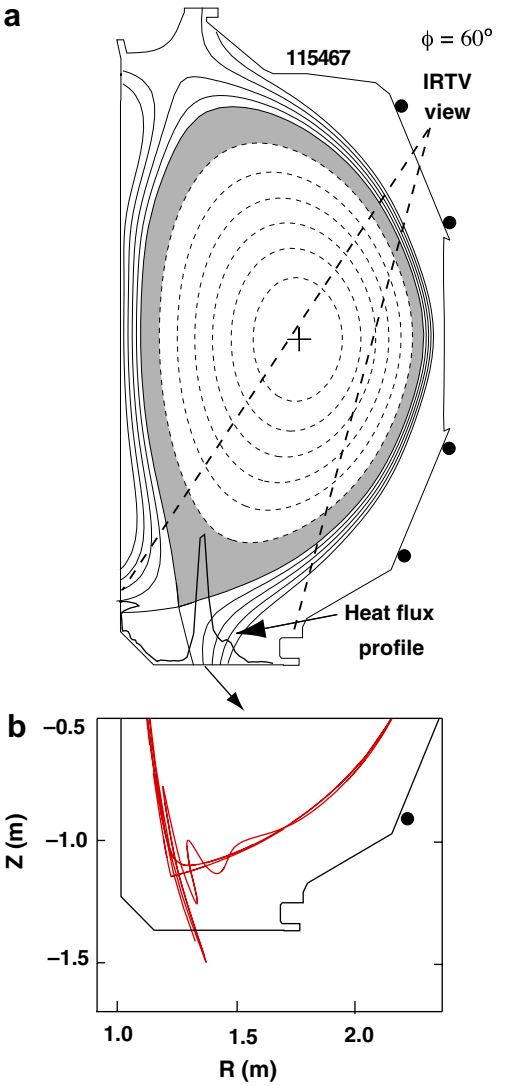

Fig. 1. (a) DIII-D axisymmetric equilibrium during discharge 115467 showing the IRTV camera view at $\phi = 60°$ and a typical heat flux profile before the I-coil (black dots) is pulsed and (b) typical non-axisymmetric separatrix structure during the I-coil pulse.

divertor as a function of time. A typical heat flux profile along the lower divertor tiles during an H-mode with edge localized modes (ELMs) and no externally imposed resonant magnetic perturbations, other than intrinsic field-errors, is shown in Fig. 1(a). The D_α camera provides 3D (R, z, ϕ) images of the lower divertor recycling with a 33 ms integration time. Fig. 1(b) shows the poloidal structure of the split separatrix at $\phi = 60°$ calculated with TRIP3D_MAP during an $n = 3$ I-coil pulse. This calculation is done using the methods described in Refs. [1,6] and with an I-coil perturba-

tion field that is approximately the same size as the field-error perturbations at the unperturbed separatrix.

The key plasma parameters for this discharge are: elongation (κ) of 1.8, upper and lower triangularities of 0.35 and 0.73 respectively, toroidal magnetic field $B_T = 1.6$ T, plasma current $I_p = 1.1$ MA and neutral beam heating power of 5.1 MW. The electron pedestal density normalized to the Greenwald density ($n_{e,ped}/n_G$) is 0.55 with a line averaged density (n_e) of 7.2×10^{19} m^{-3}. An L–H transition occurred at $t = 1600$ ms and established regular Type-I ELMs within the first 300–400 ms of the L–H transition. The safety factor at the 95% flux surface (q_{95}) is 3.7. In this discharge an $n = 3$ I-coil pulse was used to suppress ELMs [9] and the DIII-D C-coil was not used. Divertor Langmuir probe measurements indicate that the inner divertor leg is detached and the outer leg is close to detachment [12]. The properties of the discharges during the ELM suppressed phases along with various diagnostic responses to the I-coil pulse are discussed extensively in Refs. [9,13,14].

Data collected with the IRTV shows a distinct change in the divertor heat flux at the beginning of the I-coil current pulse followed by the formation of two distinct peaks that are slowly modulated during the remainder of the pulse. This temporal evolution of the divertor heat flux across the outer strike point region is represented using contour lines in Fig. 2(a). Here, red[1] indicates a heat flux of approximately 20 W/cm^2 and each additional contour line represents a change of 5 W/cm^2. A 4.4 kA, $n = 3$, I-coil current pulse is initiated at 3.0 s and terminates at 4.4 s. The heat flux profile evolves from a single peaked structure at $t = 2.9$ s, as shown by the solid green 'I-coil off' profile in Fig. 2(b), to a double peaked profile at $t = 3.3$ s with the 'I-coil on' as shown by the red dashed profile in Fig. 2(b). The maximum peak-to-peak separation of the double peak formation is 55 mm.

A splitting of the D_α recycling emission near the outer strike point is also seen when the I-coil is pulsed in this discharge. Fig. 3 shows the D_α TV view 60 ms after the initiation of the I-coil pulse. The radial resolution of the camera at the toroidal tangency point with the outer strike point ($\phi = 195°$) is 5 mm in this view. The peak-to-peak splitting of the recycling in this image is estimated to be between 20 and 30 mm at $\phi = 195$ °. In addition the full width of each peak is estimated to be between 10 and 20 mm.

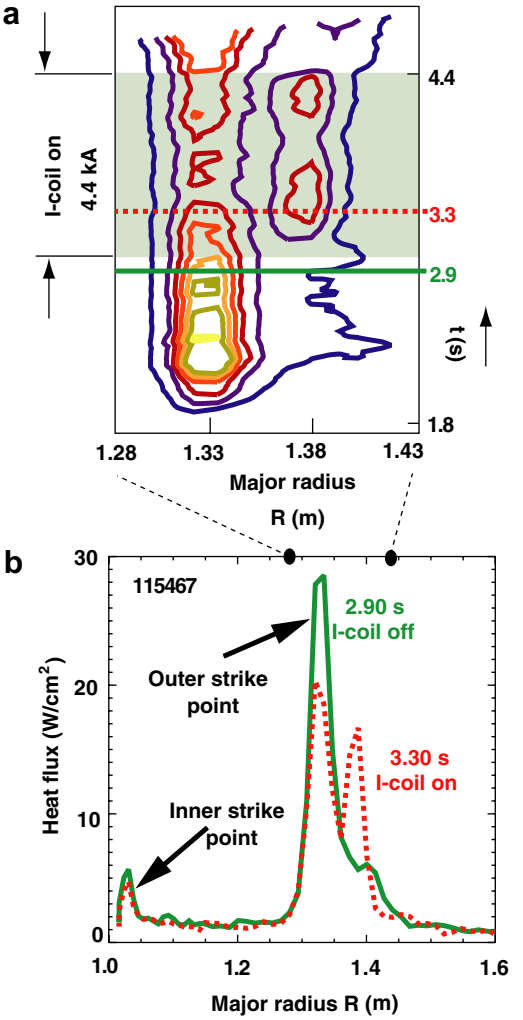

Fig. 2. (a) Contour plot showing the radial distribution of the lower divertor heat flux near the outer strike point ($R = 1.31$ m) as a function of time in discharge 115467. The I-coil is pulsed to 4.4 kA between 3.0 s and 4.4 s and (b) radial heat flux profiles just before (2.9 s) and during (3.3 s) the I-coil pulse.

3. Numerical modeling

Numerical modeling of the magnetic footprint near the outer strike point before the I-coil pulse in discharge 115467 shows a small $n = 1$ split peak pattern at $\phi = 195°$ with a peak-to-peak separation of approximately 5 mm as seen in Fig. 4. This splitting is due to measured non-axisymmetric intrinsic

[1] For interpretation of the references to colour in this figure, the reader is referred to the web version of this article.

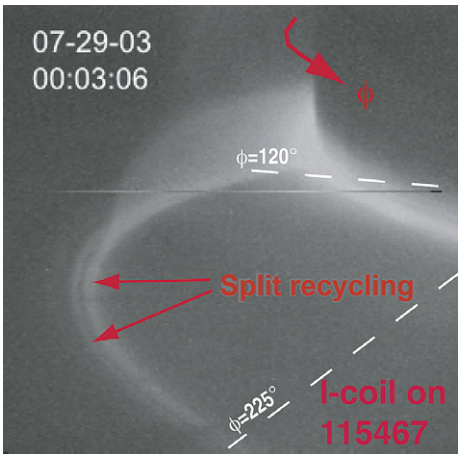

Fig. 3. Lower divertor D_α recycling emission splits along the outer strike point during the I-coil pulse in discharge 115467.

field-error components generated by the vertical field coils (DIII-D f-coils), the toroidal field coil bus bars and the toroidal field coil center post legs. The TRIP3D code uses engineering quality models of the known field-errors and perturbation coils (i.e., the C- and I-coils) in DIII-D to calculate magnetic field vectors needed for field line integration studies [5]. The data shown in Figs. 4 and 5 are accumulated by following $\sim 1.4 \times 10^4$ field lines started at 180 uniformly distributed poloidal points on 10 unperturbed normalized flux surfaces between $\psi_N = 0.98$ and 0.998 and 8 uniformly distributed toroidal angles. Each field line is integrated along the toroidal field direction for 200 toroidal transits or until it strikes the lower divertor target plate where its position is recorded with a dot and its flux surface of origin is designated by the color of the dot used with red to blue corresponding to 0.98–0.998 respectively.

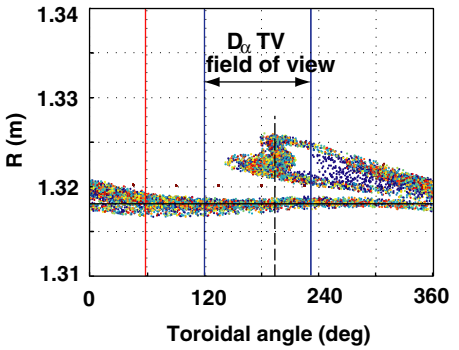

Fig. 4. Magnetic footprint calculated with TRIP3D showing field line strike point locations in (R, ϕ) due to DIII-D field-errors only (before the I-coil is pulsed) in discharge 115467.

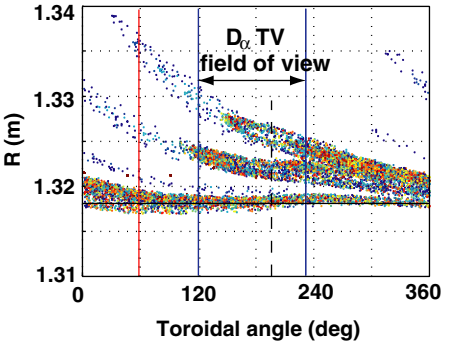

Fig. 5. The same as Fig. 4 during the 4.4 kA $n = 3$ I-coil pulse in discharge 115467.

With the I-coil on in discharge 115467 the magnetic footprint calculated with TRIP3D forms a clear $n = 3$ structure as can be seen along a toroidal cut through $R = 1.325$ m in Fig. 5. The width of the structure at $\phi = 195°$ remains approximately constant as seen in Fig. 5 compared to the field-error width shown in Fig. 4. At the location of the IRTV ($\phi = 60°$ indicated by the red line in Figs. 4 and 5) three new radial stripes with peak-to-peak separations of 2 mm, 5 mm and 9 mm appear. The tips of these stripes have a much lower field line density than their base and are dominated by field lines from flux surfaces just inside the unperturbed separatrix.

4. Discussion and conclusions

A comparison of the experimental data, during the I-coil pulse as shown in Figs. 2 and 3, with the numerical calculations of the magnetic footprint near outer strike point (Fig. 5) indicates that a non-axisymmetric splitting of the separatrix is qualitatively consistent with the experimental data. Since the structure appears in both the heat flux profile at $\phi = 60°$ and in the D_α images at $\phi = 195°$ when the I-coil pulse is initiated and disappears when the I-coil pulse terminates it is clearly correlated with the applied $n = 3$ magnetic perturbation. Similar features have been seen during locked modes, ELMs and disruptions in DIII-D [1,15].

Quantitative estimates of the peak-to-peak splitting in the heat flux profile determined from IRTV indicate two peaks separated by 55 mm while the numerical modeling results indicate a total of four

discrete radial stripes separated by 2, 5 and 9 mm from inner to outer respectively, approximately 20 mm in total. Since the spatial resolution of the IRTV is of order 15 mm the fine structure predicted by the modeling may not be visible in the measured data. The data and the modeling taken together suggest that the applied perturbation may be amplified by as much a factor of 2–3 by plasma effects. Interestingly, at the D_α imaging location the numerical modeling results indicate a peak-to-peak splitting of about 8–15 mm during the I-coil pulse and the experimental data shows a 20–30 mm split which would also be consistent with an amplification factor of 2–3. Additionally, the decrease seen in the experimental peak-to-peak separation from $\phi = 60°$ to $\phi = 195°$ is qualitatively consistent with the numerical results shown in Fig. 5. Future studies will examine the relationship between the magnitude divertor heat flux inside the magnetic footprints and the structure of the edge stochastic layer as previously done in limiter tokamaks [16,17].

These results demonstrate that heat and particle deposition patterns seen on the target plates of a poloidally diverted plasma are qualitatively consistent with the magnetic footprints produced by a splitting of the separatrix when small non-axisymmetric magnetic perturbations are present. In addition, the experimental data presented here indicate that the plasma response may amplify the magnitude of the splitting by as much as a factor of 3 and that small non-axisymmetric perturbations, when combined with the potential for plasma amplification, may have significant implications for divertor designs in burning plasma devices such as ITER.

Acknowledgement

This work was supported by the US Department of Energy under DE-FC02-04ER54698, DE-FG02-04ER54758, and W-7405-ENG-48.

References

[1] T.E. Evans, R.K.W. Roeder, J.A. Carter, et al., J. Phys.: Conf. Ser. 7 (2005) 174.
[2] J. Guckenheimer, P. Holmes, Appl. Math. Sci., 42, Springer-Verlag, New York, 1983.
[3] V.K. Melnikov, Transactions of Moscow Mathematical Society 12 (1963) 1.
[4] J.D. Meiss, Rev. Mod. Phys. 64 (1992) 795.
[5] T.E. Evans, R.A. Moyer, P. Monat, Phys. Plasmas 9 (2002) 4957.
[6] R.K.W. Roeder, B.I. Rapoport, T.E. Evans, Phys. Plasmas 10 (2003) 3796.
[7] L.L. Lao, H.E.St. John, R.D. Stambaugh, et al., Nucl. Fus. 25 (1985) 1611.
[8] S.S. Abdullaev, K.H. Finken, M. Jakubowski, M. Lehnen, Nucl. Fus. 46 (2006) s113.
[9] T.E. Evans, R.A. Moyer, P.R. Thomas, et al., Phys. Rev. Lett. 92 (2004) 235003.
[10] C.J. Lasnier, D.N. Hill, T.W. Petrie, et al., Nucl. Fus. 8 (1998) 1225.
[11] M.E. Fenstermacher et al., Rev. Sci. Instrum. 68 (1997) 974.
[12] J.G. Watkins, T.E. Evans, et al., J. Nucl. Mater., in press, doi:10.1016/j.jnucmat.2007.01.064.
[13] T.E. Evans, R.A. Moyer, J.G. Watkins, et al., Nucl. Fus. 45 (2005) 595.
[14] R.A. Moyer, T.E. Evans, T.H. Osborne, et al., Phys. Plasmas 12 (2005) 056119.
[15] T.E. Evans, C.J. Lasnier, D.N. Hill, et al., J. Nucl. Mater. 220&222 (1995) 235.
[16] Ph. Ghendrih, A. Grosman, J. Nucl. Mater. 241&243 (1997) 517.
[17] M.W. Jakubowski, O. Schmitz, S.S. Abdullaev, et al., Phys. Rev. Lett. 96 (2006) 035004.